Cell, Vol. 108, 83–96, January 11, 2002, Copyright ©2002 by Cell Press

Nuclear Envelope Breakdown Proceeds by Microtubule-Induced Tearing of the Lamina

Joël Beaudouin,[1] Daniel Gerlich,[2] Nathalie Daigle,[1] Roland Eils,[2] and Jan Ellenberg[1,3]

[1] Gene Expression and Cell Biology/Biophysics Programmes
European Molecular Biology Laboratory
D-69117 Heidelberg
Germany

[2] Intelligent Bioinformatics Systems
German Cancer Research Center
D-69120 Heidelberg
Germany

Summary

The mechanism of nuclear envelope breakdown (NEBD) was investigated in live cells. Early spindle microtubules caused folds and invaginations in the NE up to one hour prior to NEBD, creating mechanical tension in the nuclear lamina. The first gap in the NE appeared before lamin B depolymerization, at the site of maximal tension, by a tearing mechanism. Gap formation relaxed this tension and dramatically accelerated the rate of chromosome condensation. The hole produced in the NE then rapidly expanded over the nuclear surface. NE fragments remaining on chromosomes were removed toward the centrosomes in a microtubule-dependent manner, suggesting a mechanism mediated by a minus-end-directed motor.

Introduction

The result of the G2/M transition in higher eukaryotic cells is a highly regulated switch in chromosome compartmentalization. Nuclear membranes that surround chromosomes in interphase are replaced by cytoplasmic spindle microtubules which organize and segregate chromosomes in an "open" mitosis. A key step of the G2/M transition which commits a cell to M phase is the breakdown of the nuclear envelope (NE). This structure consists of two concentric membranes, the inner (INM) and outer nuclear membrane joined at nuclear pore complexes (NPCs) and in direct continuity with the endoplasmic reticulum (ER) (Gerace and Burke, 1988). While the INM contains a unique set of transmembrane proteins, the outer is functionally equivalent to the ER and freely accessible for ER membrane proteins. Spanning both membranes are NPCs that form aqueous channels which allow selective traffic between nucleus and cytoplasm and impose a permeability barrier to free diffusion at ~40 kDa. In multicellular eukaryotes, the NE is stabilized by the nuclear lamina, a tight mesh of intermediate filament proteins underlying the inner nuclear membrane (Gruenbaum et al., 2000). Mutual molecular interactions between these structural components of the NE and heterochromatin have been demonstrated (reviewed in Goldberg and Allen, 1995; Wilson, 2000), and together with in vivo observations suggest that the nuclear periphery is a highly crosslinked and stable protein network (Daigle et al., 2001). In dividing cells, this network is abolished during NE breakdown (NEBD), which defines the transition from prophase to prometaphase in the cell division cycle (Alberts, 1994). The mechanism of NEBD has not been established. Based on indirect evidence, two models are prevalent in the literature: NE vesiculation preceded by lamina phosphorylation and NE piercing by spindle microtubules. We will briefly discuss the evidence for both hypotheses.

It is clear from biochemical studies that many NE proteins are subject to mitotic phosphorylation by MPF kinase $p34^{cdc2}$. This is believed to abolish protein-protein interactions essential for NE integrity and lead to dispersal of all major NE structural components. Nuclear lamins are phosphorylated by $p34^{cdc2}$, resulting in their depolymerization (Peter et al., 1990, 1991; Ward and Kirschner, 1990) and dispersal in mitotic cells (Daigle et al., 2001; Gerace and Blobel, 1980; Stick et al., 1988). Moreover, lamins lacking cdc2 phosphorylation sites prevent lamina disassembly (Heald and McKeon, 1990). Although it has been shown in vitro that lamin solubilization can occur in the absence of the nuclear membrane breakdown (Newport and Spann, 1987) lamin depolymerization is still thought to be necessary to disassemble nuclear membranes. NPC components have similarly been shown to become phosphorylated by $p34^{cdc2}$ (Favreau et al., 1996; Macaulay et al., 1995), presumably leading to their release from the pore complex and dispersed localization observed in mitotic cells (Daigle et al., 2001; Yang et al., 1997; Belgareh et al., 2001). INM proteins have also been shown to be mitotically phosphorylated (Courvalin et al., 1992; Foisner and Gerace, 1993; Pfaller et al., 1991), but their fate is still controversial. The generally accepted concept is that phosphorylation of lamins is a prerequisite to destabilize the NE whose membranes then vesicularize extensively (Alberts, 1994; Marshall and Wilson, 1997). While membrane vesicles enriched in INM proteins can be isolated from fractions of cell homogenates (Buendia and Courvalin, 1997; Drummond et al., 1999; Sasagawa et al., 1999), there is now good evidence that nuclear membrane proteins reside in the ER in metaphase cells (Daigle et al., 2001; Ellenberg et al., 1997; Yang et al., 1997), which itself remains an intact network in mitosis (Ellenberg et al., 1997; Terasaki, 2000; Zaal et al., 1999). A mechanism by which mitotic phosphorylation of NE proteins leads to NEBD has not been established to date, but recent studies in starfish oocytes have proposed pore complex disassembly as a possible trigger for permeabilization (Terasaki et al., 2001).

NE structure is also affected by mitotic microtubules nucleated from centrosomes in late G2/early prophase. Classic EM studies reported an intimate connection of spindle microtubules and NE in HeLa (Paweletz and Lang, 1988; Robbins and Gonatas, 1964) and plant cells (Bajer and Molé-Bajer, 1969), as well as deep pocket-like distortions of the NE in the centrosomal regions

[3] Correspondence: jan.ellenberg@embl-heidelberg.de

prior to NEBD (Robbins and Gonatas, 1964). More recently, the reinvestigation of these structures in mammalian cells by immunofluorescence has led to the proposal of microtubule piercing as the mechanism for NEBD (Georgatos et al., 1997), but no direct evidence for this hypothesis has emerged so far. Additionally, there are indications that the minus-end-directed microtubule motor dynein localizes to the NE of mammalian cells and *C. elegans* embryos in prophase (Busson et al., 1998; Gönczy et al., 1999). Dynein is required for attachment of centrosomes to the NE both in *C. elegans* and *Drosophila* (Gönczy et al., 1999; Robinson et al., 1999). The function of this interaction has been interpreted to be centrosome positioning and separation, supported by studies of mutant dynein in *Dictyostelium* (Ma et al., 1999). In *Xenopus* extracts, dynein is responsible for nuclear movements, similar to female pronuclear movements after fertilization in many oocytes (Reinsch and Gönczy, 1998). Moreover, in *S. pombe*, dynein is required for nuclear movements in meiotic prophase (Yamamoto et al., 1999), and it is essential in filamentous fungi for the invasion of nuclei into the tip of hypha before mitosis (Plamann et al., 1994). Despite the many lines of evidence for a microtubule-NE interaction at the G2/M transition, it has not been established if a mechanistic connection exists between mitotic microtubules and NEBD, and what the nature of such a connection could be.

In this study, we investigated the mechanism that leads to NEBD in living cells. The behavior of two INM proteins, a nucleoporin, a B type lamin, α-tubulin, and chromosomes was analyzed in mammalian cells during G2/M transition. Because of the spatiotemporal complexity of mitosis, we used quantitative 4D imaging (Gerlich et al., 2001) combined with fluorescence photobleaching techniques (Ellenberg and Lippincott-Schwartz, 1997) to analyze events during NEBD. Our results lead us to propose a mechanism for NEBD in which microtubule-induced tearing of the nuclear lamina causes nuclear permeabilization.

Results

Dynamics of Microtubules, NE, and Chromosomes at the G2/M Transition

In this study, we use a mammalian cell system to analyze NEBD in vivo using multicolor confocal 4D imaging to obtain a direct space-time correlation of two proteins in the same dividing cell (Gerlich et al., 2001). To precisely determine the time point of nuclear permeabilization, we measured the influx of large cytoplasmic molecules or the appearance of the first discontinuity in the NE. These events serve to define NEBD for the purpose of this study and are used as a temporal reference to correlate different G2/M processes. To ensure that the resolution of the 4D imaging system was sufficient to detect the initial gaps associated with nuclear permeabilization, we observed the influx of 500 kDa cytoplasmic dextran through the lamina. As shown in Figure 1A, single holes could be detected at the start of the dextran influx, demonstrating that they are valid temporal markers of NEBD. Importantly, a dextran wave entered through the gap (Figure 1A, 0:00) which thus also marked the site of permeabilization, consistent with previous results in starfish oocytes (Terasaki et al., 2001).

Next, the distinct morphological stages of G2/M transition from early prophase until metaphase were characterized in NRK cells expressing proteins of the NE (lamin B receptor, LBR; lamina associated polypeptide β, LAP2β; pore membrane protein 121 kDa, POM121; lamin B1), spindle apparatus (α-tubulin), and chromosomes (histone 2B, H2B) tagged with several spectrally distinguishable fluorescent proteins (CFP, GFP, YFP; see Experimental Procedures). The earliest indication of exit from G2 was the appearance of folds in the NE close to centrosomes up to one hour prior to NEBD (not shown). ~20 min before NEBD, centrosomes separated and started to migrate apart with well formed mitotic asters. At the same time, chromosomes started to condense and appeared as defined structures at the NE (Supplemental Figure S1A; see Supplemental Data section below). NE folds then matured into invaginations severely distorting the NE (Figure 1C). Finally, the nucleus was permeabilized, evidenced by the influx of cytoplasmic molecules (Figure 1A) and the appearance of gaps in the nuclear rim (Figures 1A–1D, arrowheads; see also Supplemental Figure S1). After gap formation, chromosomes rapidly completed their condensation and congressed toward the metaphase plate while remnants of NE proteins remained associated with centrosomes until early metaphase (Supplemental Figures S1A, S1C, and S1D).

LAP2β, POM121, and Lamin B1 Remain Bound in the NE until NEBD

To address the question of whether lamin depolymerization was a prerequisite for nuclear membrane disassembly, we investigated how the kinetics of NE protein dispersion were correlated to NEBD. The redistribution of the INM protein LBR-YFP into the ER consistently started ~8 min before NEBD, with the majority of the protein already residing in the ER at the time of permeabilization (Figures 1B and 1F). The nuclear rim concentration of LAP2β, POM121, and lamin B1, however, was unchanged at the time the first gap appeared in the NE, and their dispersal started only after the nucleus was permeabilized (Figures 1C and 1D; Supplemental Figure S2A). Importantly, no soluble lamin B1 could be detected before NEBD with a sensitivity of better than 5% of the total cellular protein (Figure 1G). After NEBD, lamin B1 was solubilized rapidly within 5–10 min, and the transmembrane proteins POM121 and LAP2β equilibrated with the ER over a similar time course (Figures 1G and 1H; Supplemental Figure S2E). These results demonstrate that except for LBR, all NE proteins tested, including B type lamins, were dispersed only after NEBD. All three nuclear membrane proteins equilibrated with the ER, while lamin B1 appeared to be soluble in the cytoplasm, consistent with our previous results (Ellenberg et al., 1997; Daigle et al., 2001).

Since solubilization of the lamina was not detected prior to NEBD in intact cells, we investigated whether exchange of subunits in and out of the lamin polymer was increased in prophase. Using fluorescence recovery after photobleaching (FRAP), we have shown in the past that B type lamins are stably bound in the nuclear enve-

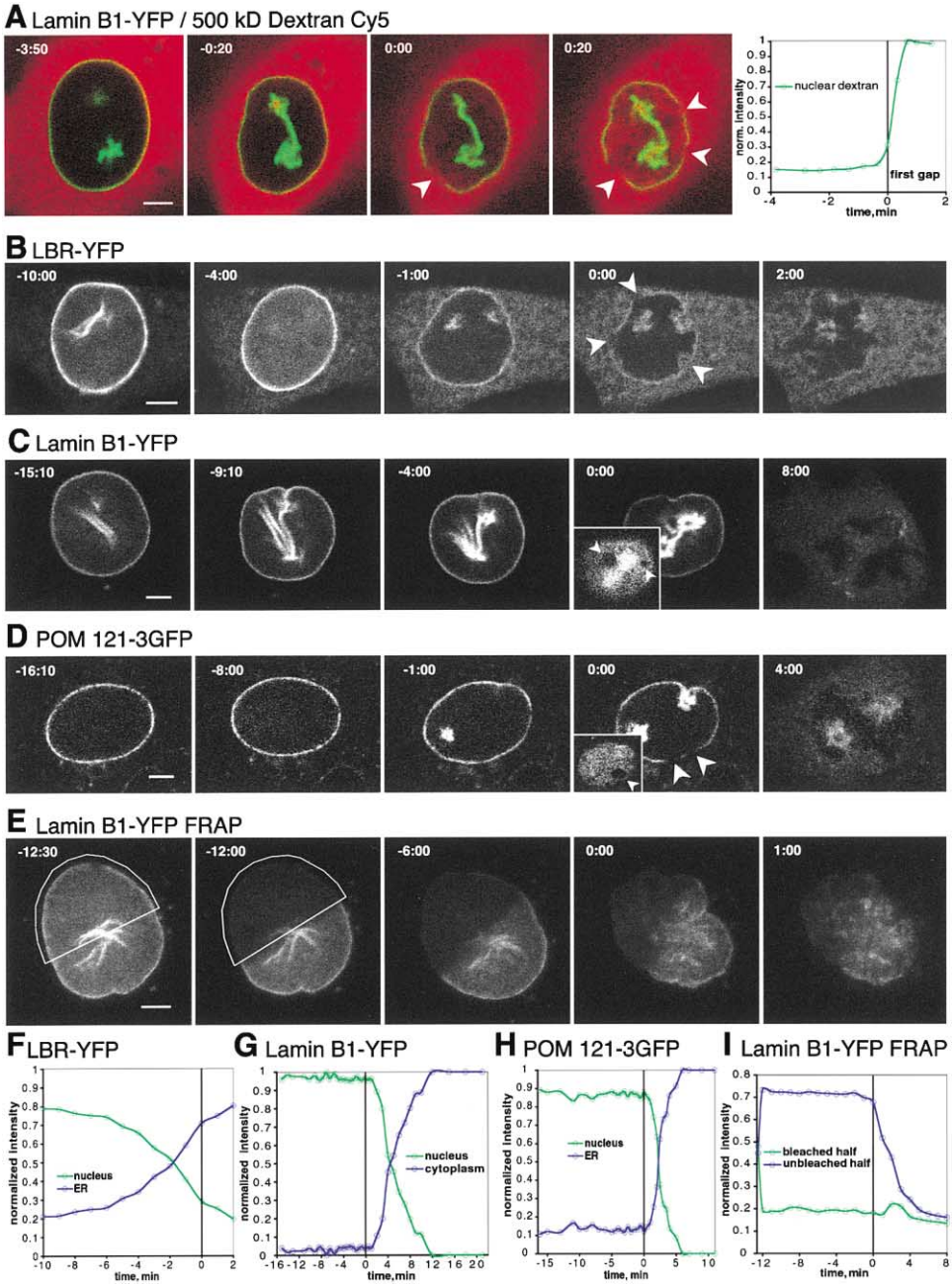

Figure 1. Fate of LBR, Lamin B1, and POM121 before and after NEBD

(A)–(E) Time is min:s; Bar: 5 μm.

(A) NEBD definition: NRK cell transiently expressing Lamin B1-YFP (green) injected in prophase with 500 kDa Cy5 dextran into the cytoplasm (red). Arrowheads show the holes on the rim. Note that a big hole is already on the rim while dextran starts entering. Also note that a wave of dextran is starting to diffuse inside the nucleus from the hole (time 0:00). See also Supplemental Movie S1A (see Supplemental Data section below). The plot shows fluorescence intensity inside the nucleus over time, normalized to 1 after NEBD. Time 0 refers to the first hole on the rim.

(B)–(D) LBR diffuses into the ER before NEBD, while lamin B1 and POM121 remain in NE until NEBD. $NRK_{LBR\text{-}YFP}$ (B), NRK transiently expressing lamin B1-YFP (C), or POM121-3GFP (D) followed by 4D imaging from prophase to prometaphase. A single section centered in the nucleus is shown. Insets in (C) and (D) show the lower nuclear surface. See also Supplemental Movie S1C for the distortion of the nucleus. Arrowheads show the first holes on the rim.

(E) Lamin B1 is immobile before NEBD. Cells as in (C). The solid line boxed region was bleached in prophase and recovery was followed until after NEBD by 4D imaging. A top projection is shown.

(F)–(H) Plots represent total intensities in the ER for LBR-YFP and POM121-3GFP ([F] and [H], blue) or in the cytoplasm for lamin B1-YFP ([G], blue) and in the nuclear rim ([F]–[H], green) for all three proteins, normalized to the total cellular intensity as 1.

(I) Plot shows total intensities of bleached and unbleached halves for lamin B1-YFP normalized to the total cellular intensity. The increase of the normalized intensity in the unbleached half between the first and second time points is due to a decrease of the total cellular intensity with the photobleaching, while the unbleached half intensity has stayed constant.

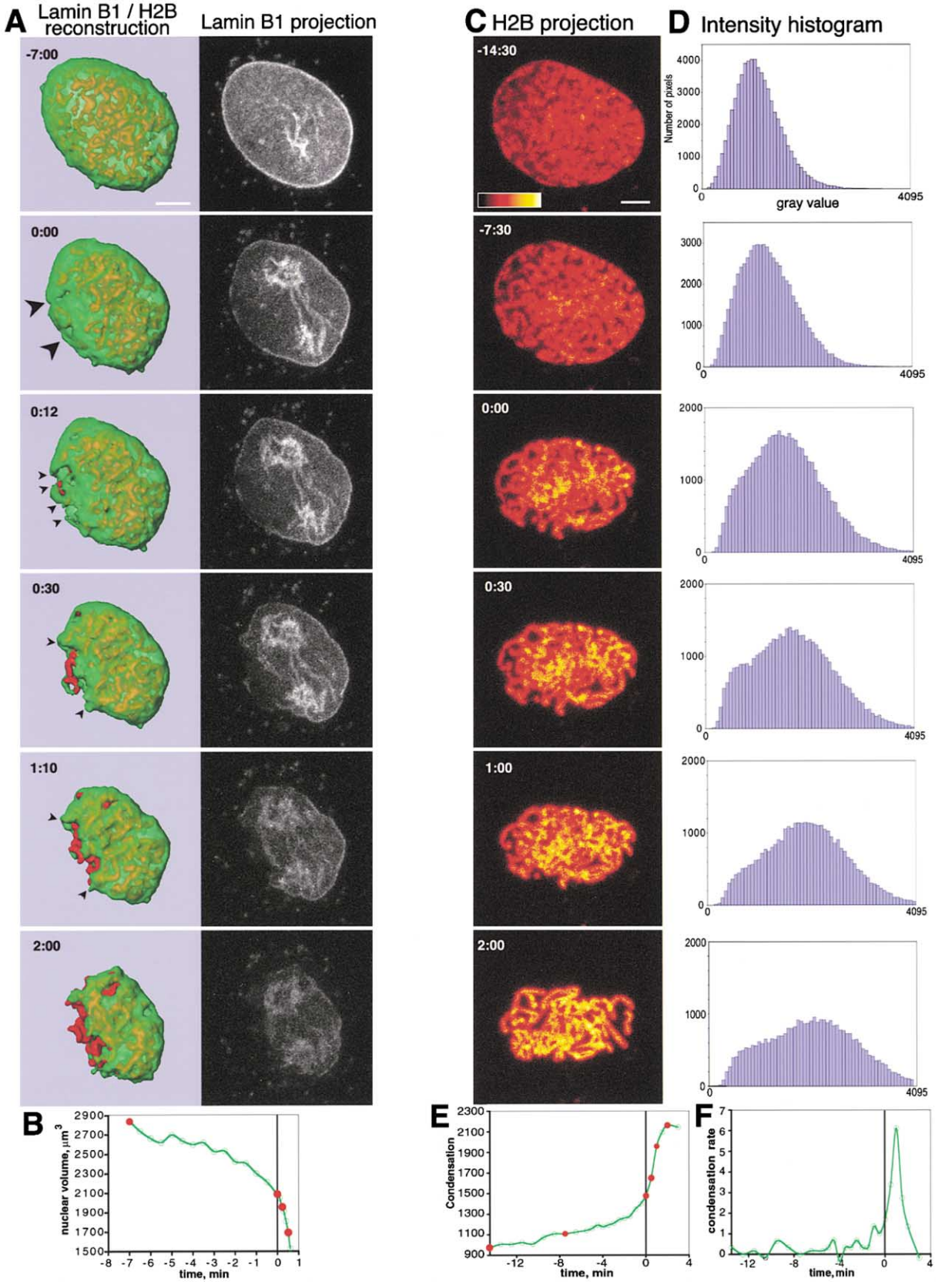
A
Lamin B1 / H2B reconstruction
Lamin B1 projection
-7:00
0:00
0:12
0:30
1:10
2:00
C H2B projection
-14:30
-7:30
0:00
0:30
1:00
2:00
D Intensity histogram
Number of pixels
gray value
4095
B
nuclear volume, μm3
time, min
E
Condensation
time, min
F
condensation rate
time, min

lope for many hours in interphase cells (Daigle et al., 2001). FRAP of lamin B1 performed on both the upper and lower nuclear surface 5–10 min before NEBD showed that lamin B1 did not recover any fluorescence, showing that the turnover of the lamin B1 was not increased (Figures 1E and 1I). FRAP in prophase cells was then applied to measure exchange from binding sites for LBR, LAP2β, and POM121, all of which are known to be strongly immobilized in interphase nuclei (Ellenberg et al., 1997; Rolls et al., 1999; Daigle et al., 2001). As in the 4D imaging experiments, the behavior of LAP2β and POM121 was indistinguishable from that of lamin B1 in that they did not show any recovery of fluorescence prior to NEBD (Supplemental Figures S2C, S2D, S2G, and S2H). Only LBR quickly recovered fluorescence in prophase with a $t_{1/2}$ of ~30 s (Supplemental Figures S2B and S2F), consistent with its early release into the ER. Our data shows that—with the exception of LBR—the NE protein network consisting of lamins, NPCs, and INM proteins remained intact until NEBD.

NEBD Results from a Single Hole which Expands Rapidly over the Nuclear Surface

Next, we investigated the precise structural nature of the permeabilization event by high resolution 4D imaging of lamin B1 and chromosomes. Quantitative reconstruction and dynamic visualization of such sequences showed that NEBD starts with one to three holes in the surface of the nuclear lamina (Figure 2A reconstruction, compare Figures 1A–1D). In all the cells observed (n = 28), the hole formed in a region of the NE not in contact with chromosomes and distal from the centrosomes, whose position was evident from the distortions of the lower surface of the nuclear lamina (Figure 2A projection). Once a hole opened, it expanded rapidly over the nuclear surface (Figure 2A, reconstruction). Hole formation occurred simultaneously for the nuclear lamina and INM or nuclear pores as determined in cells coexpressing lamin B1 with LBR/POM121 (Figures 3A and 3B). In quantitative 4D analyses of the lamina, the appearance of gaps was directly compared with the change of inferred nuclear volume (see Experimental Procedures). Hole formation reproducibly coincided with a rapid decrease in nuclear volume (Figure 2B), suggesting a link between permeabilization and nuclear shrinking. To investigate if nuclear shrinking after NEBD could be caused by condensing chromatin, we also quantitated chromosome condensation during G2/M transition from

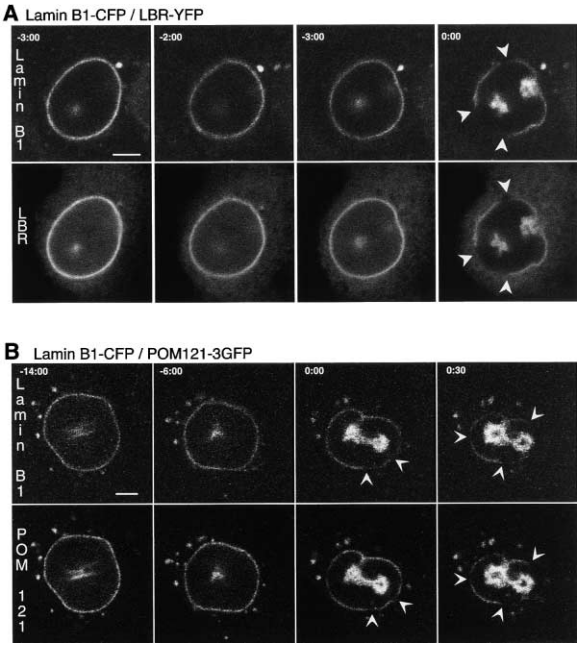

Figure 3. Holes Form Simultaneously in the Inner Nuclear Membrane, Pore Complex Network, and Nuclear Lamina

(A) and (B) Time is min:s, 0 = NEBD. Bar: 5 μm.

(A) $NRK_{LBR\text{-}YFP}$ transiently expressing lamin B1-CFP observed by 4D imaging until NEBD. Arrowheads show gaps in the nuclear rim. Note the simultaneous appearance of holes for both proteins.

(B) NRK transiently coexpressing POM121-3GFP and lamin B1-CFP observed by 4D imaging until NEBD. Arrowheads show gaps in the nuclear rim. Note the simultaneous appearance of holes for both proteins.

4D imaging experiments. As can be seen in Figures 2C–2F, chromosome condensation progressed gradually before NEBD (Figure 2E). Immediately after permeabilization, the condensation rate dramatically increased more than 3-fold and maximum condensation was reached within ~2–3 min (Figure 2F). The close correlation with nuclear shrinking (Figures 2B and 2E) suggests that the increased condensation rate triggered by NEBD provides a driving force for nuclear shrinking.

Microtubules Cause Deep Invaginations into the NE prior to NEBD

Hole formation in the lamina could be explained by two alternative but not necessarily exclusive mechanisms.

Figure 2. NEBD Starts with a Single Expanding Hole in the Lamina and Accelerates Chromosome Condensation

(A) and (C) Time is min:s, 0 = NEBD. Bar: 5 μm.

(A) $NRK_{H2B\text{-}CFP}$ transiently expressing lamin B1-YFP observed by 4D imaging during NEBD. (Left) Reconstruction of H2B-CFP (red) and lamin B1-YFP (green). Cytoplasmic autofluorescence was removed manually. (Right) Projection of lamin B1-YFP. To better appreciate the spreading hole, see Supplemental Movie S2A (see Supplemental Data section below). Arrowheads at time 0:00 show the first holes. For later time points, small arrowheads show the expansion of the hole.

(B) Nuclear volume measured by segmenting and reconstructing lamin B1 signal (Experimental Procedures) plotted over time. After NEBD, volume was estimated from a reconstituted surface until holes were too large (0:30). The gradual decrease of nuclear volume before NEBD is a consequence of growing invaginations near the centrosomes. Frames from (A) are plotted in red.

(C)–(F) Chromatin condensation after NEBD. Pseudocolor representation of maximum intensity projection of H2B-CFP, stably expressed in an NRK cell cytoplasmically injected with 500 kDa dextran (C). See also Supplemental Movie S2C. The intensity histogram of each image is plotted in (D). (E) represents the peak frequency over time, a measure of the condensation state (see Experimental Procedures). (F) represents the condensation rate defined as the first derivative of the condensation state over time. Red dots correspond to the frames from Figure 2C. Note the increase in condensation rate after NEBD, marked by the entry of 500 kDa dextran into the nucleus (not shown).

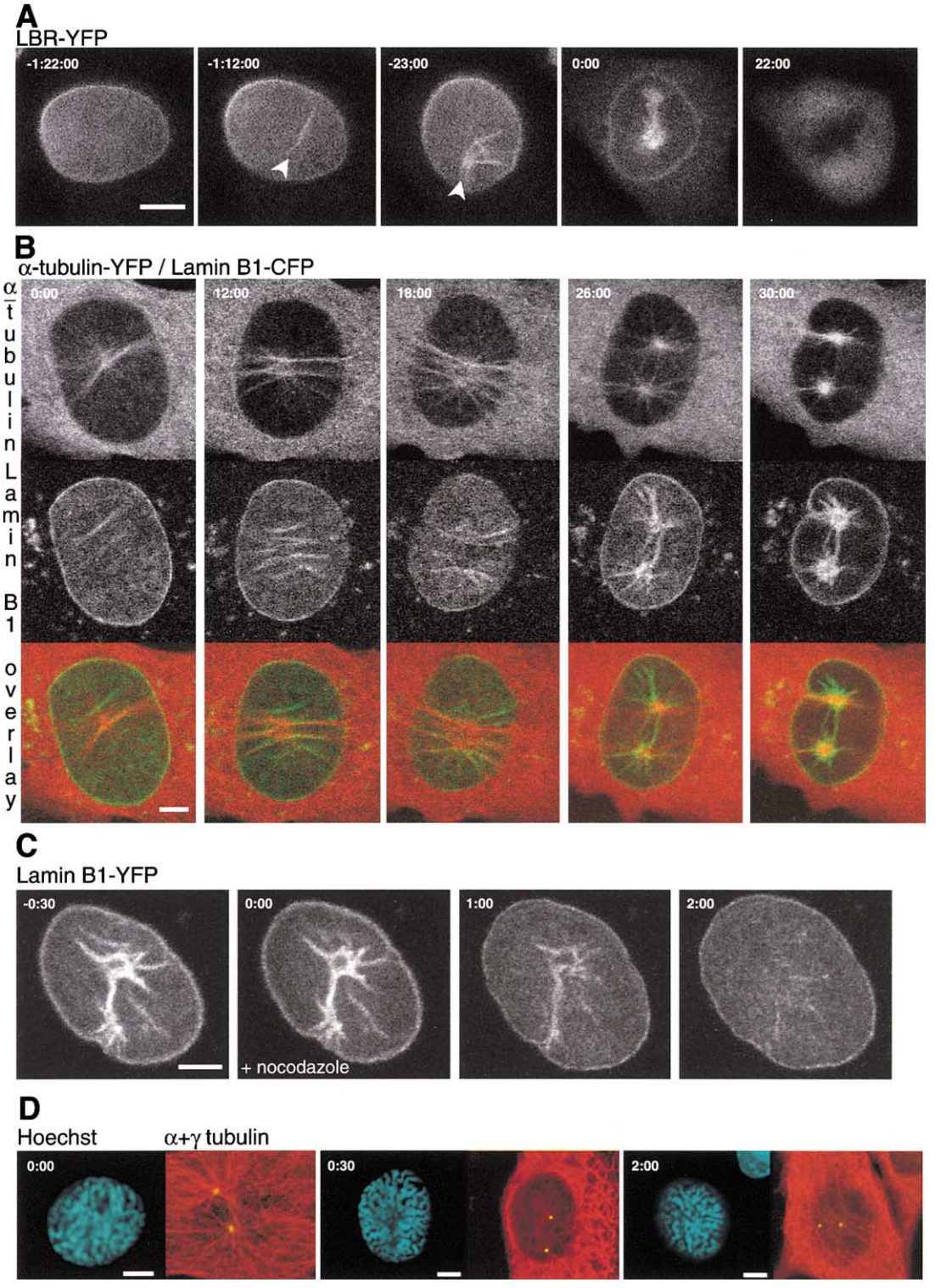

Figure 4. Microtubules Cause Reversible Invaginations of the NE in Prophase

(A)–(D) Bar: 5 μm. Time is hr:min:s

(A) Folds appear in NE up to one hour before NEBD. $NRK_{LBR\text{-}YFP}$ observed by 2D confocal time lapse from G2 to metaphase by autofocusing on the lower part of the nucleus. The dynamic appearance of folds is better appreciated in Supplemental Movie S4A (see Supplemental Data section below). Time 0 = NEBD.

(B) Centrosomally nucleated microtubule bundles colocalize with NE invaginations. See also Supplemental Movie S4B. $NRK_{\alpha\text{-}tubulin\text{-}YFP}$ cell transiently expressing lamin B1-CFP observed by confocal microscopy during prophase. The lower nuclear surface is shown.

(C) NE invaginations are reversible. See also Supplemental Movie S4C. Projection of NRK cell transiently expressing lamin B1-YFP observed by 4D imaging. 1 μg/ml nocodazole was added at t = 0.

(1) The lamin polymer could be weakened by phosphorylation-induced depolymerization prior to NEBD, and the first site to be completely disassembled would form a hole in a random position. However, the static behavior of the lamina until NEBD observed in 4D imaging and FRAP experiments, as well as the reproducible position of the hole, argued against this possibility. (2) Alternatively, the branched lamin polymer could be stretched by mechanical forces, and gaps would result from tearing of the lamina. To test the latter, we analyzed changes in NE surface prior to NEBD. In early prophase, folds and indentations appeared in both the INM and the lamina up to one hour before NEBD (Figure 4A, arrowheads). The folds eventually grew in size and depth to ~10 μm deep invaginations (Figure 4B). The indentations invariably contained the centrosomes and were later frequently connected by a bridgelike fold in the NE (Figure 4B). The strong nuclear deformation before NEBD suggested forces acting on the outside of the nucleus. To test if these forces were generated by microtubules, we treated prophase cells with nocodazole during 4D imaging experiments. NE invaginations were completely abolished within two minutes of nocodazole addition, demonstrating that they were dependent on dynamic microtubules (Figure 4C). The highly distorted NE returned to a flat spherical shape indistinguishable from late G2, demonstrating that deformation was completely reversible. Over short times, nocodazole had a selective effect on spindle microtubules in early prophase, as shown by immunofluorescence of cells fixed at different times after drug addition. Centrosomally nucleated microtubules were depolymerized within 30 s, while cytoplasmic microtubules remained intact much longer (Figure 4D). Thus, early spindle microtubules were necessary for NE invaginations.

The NE Is Torn as a Result of Tension Produced by Spindle Microtubules

Relaxation of invaginations in the prophase lamina during nocodazole treatment supported the hypothesis that the NE is under tension from spindle microtubules that are attached to its surface. To directly demonstrate tension, geometrical landmarks were created in the flat lamina of early prophase cells coexpressing lamin B1 and H2B by pattern photobleaching. A grid of 5 × 5 crossed lines could be followed by 4D imaging from early prophase until NEBD on the upper and lower nuclear surfaces (Figure 5A). The extent of tension and shearing exerted by microtubules on the intact nucleus became immediately evident. The gridlines were severely distorted near the centrosomes on the lower surface, as well as on the upper surface distal from centrosomes (Figure 5A). In addition, tracking the movement of condensing chromosomes during NE distortions revealed that the force produced by microtubules also resulted in movement of chromosomes that strictly correlated with the movement of crossed lines in the photobleached grid (Figure 5B). Thus, the position of condensing chromosomes still connected to the NE was affected by microtubules located outside the nucleus before NEBD.

Whether the distribution of tension on the lamina surface was related to the site of hole formation was investigated next. Gaps in the lamina appeared reproducibly at the site of maximum deformation of the bleached grid (Figure 5A, upper surface arrowheads), consistent with a tearing mechanism. The lamin polymer in these regions was stretched 1.5-fold, measured by the change in distance of two line intersections (Figure 5C). Conversely, on the lower nuclear surface close to the centrosomes, line intersections came closer together as a result of infolding of the NE (Figure 5A; lower surface, Figure 5D). After a hole was formed in the lamina surface opposite the centrosomes at the site of maximum stretching, the NE rapidly collapsed, relaxing the tension (Figure 5A, 0:00). Treating cells with nocodazole for longer times in early prophase profoundly changed the G2/M transition process. The NE was initially smoothed (Figure 5E, 2:20) corresponding to the depolymerization of mitotic microtubules (Figures 4C and 4D). Three min after nocodazole application, however, the entire cytoskeleton became affected, and cells started to detach from the substrate, resulting in a "crumpling" of the lamina around condensing chromosomes (Figure 5E, 3:20) followed by the appearance of soluble lamin B1. Finally, small gaps appeared at several sites situated between chromosomes and did not expand (Figure 5E, 11:40 arrowheads), and the lamin fragments between them dispersed gradually.

NE Parts Disengage from Chromosomes and Move Toward the Minus End of Spindle Microtubules

Insight into the nature of the force exerted on the NE by prophase spindle microtubules came from analyzing cells in prometaphase. After NEBD, collapse of the NE created regions devoid of ER in the cytoplasm adjacent to the nucleus (Figures 6A and 6B, arrowheads). Most likely this represented a localized opening of the dense ER network due to holes forming in the NE and/or extrusion of the nucleoplasm. While LBR had redistributed into the mitotic ER, LAP2β, lamin B1, and POM121 were still present in portions of the NE attached to chromosomes. After nuclear shrinking, these structures were moved from chromosomes toward the centrosomes in a vectorial manner (Figures 6D and 6E and Supplemental Movie S6D; see Supplemental Data section below). The movements exhibited the characteristic stop and go behavior of microtubule motor-dependent membrane movements (Presley et al., 1997), and reached peak speeds of up to 1.8 μm/s but most frequently moved at ~0.7 μm/s (n = 47, Figure 6F). The translocation added NE material to the mass already accumulated at the centrosomes by the invagination process. Lamin B1, LAP2β, and POM121 remained enriched around the centrosomes for up to 10 min after NEBD and were only completely dispersed into the ER (LAP2β, POM121) or cytoplasm (lamin B1) by early metaphase (Figures 6B

(D) Microtubules that induce NE invaginations can be depolymerized in 30 s. NRK cells were left untreated (t = 0) or fixed 30 s and 2 min after addition of 1 μg/ml nocodazole and stained for DNA (Hoechst 33342, blue), microtubules (anti-α-tubulin, red), and centrosomes (anti-γ-tubulin, green). Confocal sections containing the centrosomes are shown. Nocodazole was added at t = 0.

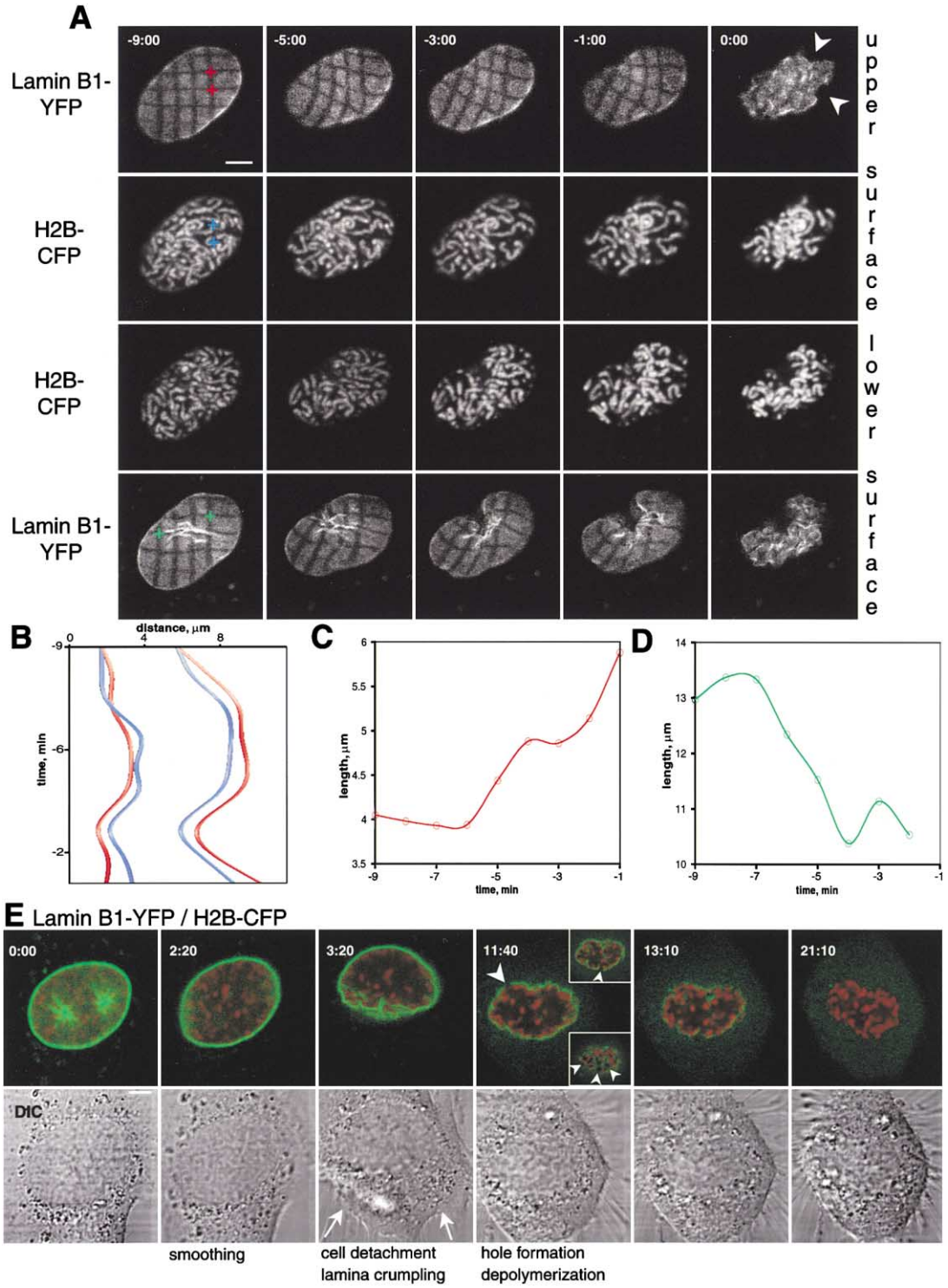

Figure 5. Microtubule-Induced Deformations Lead to Stretching and Tearing of the Lamina

(A) Grid pattern was bleached on the upper and lower surface of the lamina of $NRK_{H2B\text{-}CFP}$ cell transiently expressing lamin B1-YFP which was then followed by 4D imaging. Confocal sections containing the upper (two top rows) and lower nuclear surface (two bottom rows) are shown. Arrowheads mark the two first holes in the lamina. See Supplemental Movie S5A (see Supplemental Data section below) to better appreciate stretching. Time is min:s, 0 = NEBD. Bar: 5 μm.

(B) Space-time plot shows the positions of the two intersections marked in (A) in the lamina and on the chromosomes, tracked independently in the 4D data set. Note the correlation between chromosome and lamina movements.

(C) Distance between the two bleach line intersections on the upper nuclear surface marked red in (A) plotted over time. Note the 1.5-fold stretching within 5 min.

and 6C). Addition of nocodazole to prometaphase cells completely abolished the centrosome-directed movement of NE remnants (not shown). In this case, lamin B1 remained bound to chromosomes until its dispersal was completed (compare Figure 5E). Thus, microtubule-dependent forces continued to act on the NE after NEBD, pulling NE material in a minus-end-directed manner toward the centrosome where their dispersal was completed.

Discussion

The Fate of NE Proteins in Mitosis

Three NE proteins, LAP2β, POM121, and lamin B1, did not change the turnover from their binding sites or their localization in the NE before NEBD. These proteins were dispersed from the NE only after NEBD, suggesting that their interactions persisted in prophase. This argues against the classic model of NEBD, where mitotic phosphorylation of NE proteins and especially of the lamina globally destabilizes the NE and is required for its permeabilization. Rather, NE permeabilization itself appeared to trigger the disassembly of the stable NE protein-protein interactions. The only NE protein that showed a different behavior was LBR. It became highly dynamic in the NE before NEBD and concomitantly started to diffuse into the ER. A possible explanation for this behavior could be that LBR loses its affinity to the lamina (Ye and Worman, 1994) due to mitotic phosphorylation (Courvalin et al., 1992) in prophase, allowing it to escape into the ER. Eventually, all nuclear membrane proteins tested equilibrated with the ER in prometaphase, consistent with our earlier results (Ellenberg et al., 1997; Daigle et al., 2001). We can thus define the ER as the reservoir and means of partitioning for nuclear membrane proteins in mitosis.

Effects of Microtubule-Dependent Forces on the Nucleus

1. Reversible Deformation

Deformation of the NE close to the centrosomes was one of the earliest morphological changes accompanying entry into mitosis. Such invaginations have been described before in live sea urchin embryos (Hamaguchi et al., 1993; Longo, 1972; Terasaki, 2000) and fixed mammalian cells (Bajer and Molé-Bajer, 1969; Georgatos et al., 1997; Paweletz and Lang, 1988; Robbins and Gonatas, 1964; Zatsepina et al., 1977), and have been suggested to reflect "piercing" of the NE by spindle microtubules (Georgatos et al., 1997). We show here that permeabilization did not initiate at the invaginations, arguing against a piercing function. The rapid reversal of NE deformations upon depolymerization of spindle microtubules suggests counteracting forces. Such a force could be the elasticity of the lamina, which would tend to smooth folds after removal of microtubules. Another possibility is that cytoplasmic intermediate filaments, which have been shown to be mechanically linked to the nucleus (Maniotis et al., 1997) and appear to "suspend" the nucleus in the cytoplasm (Fey et al., 1984), could stabilize its spherical shape. The fact that nuclei crumpled in cells that detached due to three minutes of nocodazole treatment supports the notion of stabilizing cytoskeletal forces. In addition, NE deformations were detected by ER, INM, NPC, and lamin markers prior to NEBD, reinforcing the view that the NE is a crosslinked protein network (Daigle et al., 2001) that can transduce forces from the cytoplasmic to the nuclear side.

2. Stretching and Tearing of the Lamina

Surprisingly, microtubule-dependent forces not only deformed the NE but also mechanically stretched the nuclear lamina before NEBD, demonstrating pulling forces in the plane of the NE. Stretching was followed by the formation of holes in the NE at the site of maximal tension which can thus be defined as tearing. Tearing reproducibly took place distal from centrosomes, the force-producing centers. During NEBD, the chromosomes attached to the NE behaved like springs poised to condense, as their condensation rate tripled immediately after tearing. Before NEBD, these contracting forces of chromosomes would thus counteract microtubule-induced stretching of the lamina and make regions of the NE devoid of chromosomes most vulnerable to tearing. Consistent with this, the site of tearing was reproducibly in an area of the NE not in contact with chromosomes. The tearing site would thus be determined by the geometry of the mitotic spindle and chromosome-NE contacts. Only after NEBD did lamins begin to depolymerize quickly and LAP2β and POM121 were released into the ER. This suggests that NEBD triggers at least two processes: (1) The balance of forces that maintains the spherical nuclear shape is abolished catastrophically, allowing accelerated chromosome condensation which leads to nuclear shrinking; and (2) B type lamins, INM proteins, and stable nucleoporins are dispersed, presumably by massive entry of kinases or kinase-activating proteins from the cytoplasm.

3. Removal of NE Pieces from Chromosomes

Microtubules continued to act on the NE in prometaphase. Parts of the NE still attached to chromosomes were removed toward the centrosome in a vectorial, nocodazole sensitive manner. The curvilinear tracks of these movements with peak velocities of up to 1.8 μm/s are consistent with a cytoplasmic dynein-mediated process. This suggests that the same minus-end-directed motor could produce the forces leading to NE deforma-

(D) Distance between the two bleach line intersections on the lower nuclear surface marked green in (A) plotted over time. Note the decrease of distance due to folding.

(E) In nocodazole-treated cells, holes in the lamina do not expand.

Confocal section of $NRK_{H2B\text{-}CFP}$ cell transiently expressing lamin B1-YFP (upper row, see also Supplemental Movie S5E) and DIC (lower row). 1 μg/ml Nocodazole medium was added at time 0. At time 2:20, invaginations have disappeared (smoothing). At time 3:20, the cell starts detaching (see DIC, arrowhead), and crumpling of the lamina around the chromosomes appears on the same side. At time 11:40, several holes are visible (arrowheads), and depolymerization has already started. Later, depolymerization and fragmentation continues. Fragments remain connected to chromosomes (time 13:10, fluorescence). Time is min:s. Bar: 5 μm.

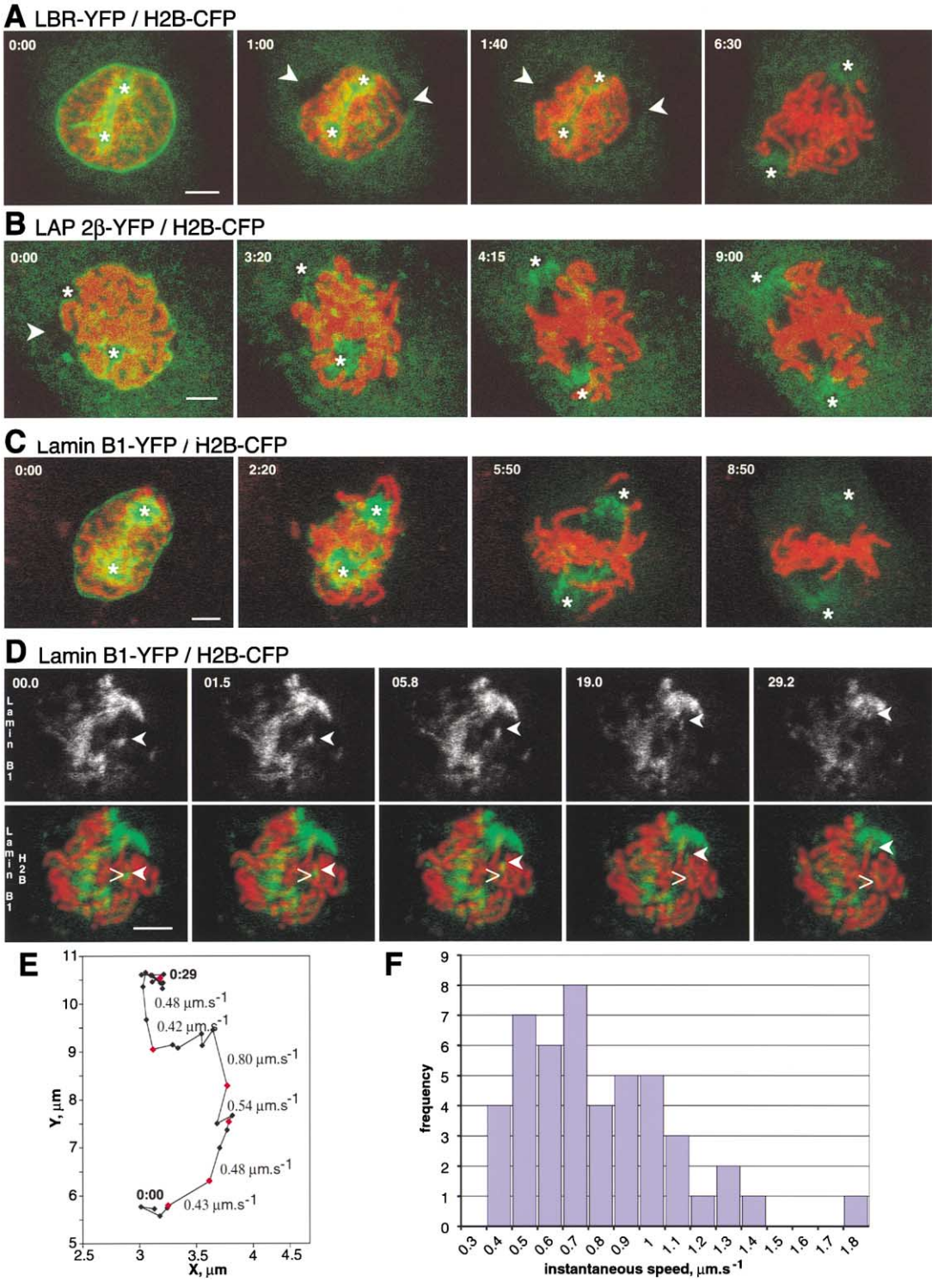

Figure 6. After NEBD, NE Parts are Pulled off Chromosomes toward the Centrosomes

(A)–(C) Projections of $NRK_{H2B\text{-}CFP}$ cells transiently expressing LBR-YFP (A), LAP 2β-YFP (B), and lamin B1-YFP (C) followed after NEBD by 4D imaging. The stars show the position of the centrosomes. Movement of NE structures is better appreciated in the corresponding Supplemental Movies S6A and S6B (see Supplemental Data section below). Time is min:s, 0 = NEBD. Bars: 5 μm.

(D) and (E) Tracking of minus-end-directed NE movements. $NRK_{H2B\text{-}CFP}$ cell transiently expressing lamin B1-YFP followed by 4D imaging. Two confocal sections are projected, the tracked fragment moves from the lower to the upper one. The upper row shows lamin B1-YFP alone and the lower row shows lamin B1-YFP (green) and H2B-CFP (red) to show that the fragment movement doesn't affect chromosome positions. Movement is better appreciated in Supplemental Movies S6D1 and S6D2. Arrowheads indicate tracked fragment; open arrowheads indicate the stationary chromosome the fragment was associated with prior to movement. Stars show position of the centrosomes. Time is in seconds.

tions before NEBD and the tearing event that permeabilized the nucleus. Dynein attached to the NE is a likely candidate to mediate microtubule-NE interactions at the G2/M transition, since it has been shown to localize to the NE in prophase (Busson et al., 1998; Salina et al., 2002). Before NEBD, forces generated in the cytoplasm were able to act on the nuclear lamina. The only known NE structure that could transduce force between cytoplasm and lamina is the immobile NPC (Daigle et al., 2001), which we speculate could serve as an attachment site for microtubules via dynein/dynactin (Salina et al., 2002). After NEBD, microtubules would remain attached to NPCs in NE fragments on chromosomes and pull them away from the chromosome surface toward the centrosomes.

Mechanical Checkpoint or Clearing of Kinetochores?

If NEBD can occur in the absence of microtubules, what then is the function of NE tearing? In the absence of microtubules, NEBD did occur—but by a different mechanism where nuclear shrinking was followed by permeabilization through many small holes that did not expand. Mitotic phosphorylation cascades are thus sufficient to drive the nucleus into disassembly even without microtubules, but this route may miss an important regulatory component. Tearing of the NE by microtubules could be a means to couple spindle assembly and NEBD in time. Only a reasonably developed spindle would produce sufficient force to rupture the stable NE protein network. This "mechanical checkpoint" would prevent breakdown of the membrane compartment before the microtubule-based spindle compartment has formed to replace it. Such a mechanism could be important to avoid loss of chromosomes due to premature NEBD.

Alternatively, the purpose of attaching microtubules to the NE could be to free the chromosome surface and especially kinetochores from the tightly attached nuclear lamina and inner nuclear membrane. The extensively crosslinked NE organization in vertebrate cells (Daigle et al., 2001) poses a problem for mitosis with exclusively cytoplasmic microtubules because large parts of the NE shield the chromosome surface from microtubules after NEBD. Phosphorylation-driven disassembly alone may not free the chromosomes efficiently enough, and in fact we observed that the majority of lamin B1, LAP2β, and POM121 were disassembled after NE fragments had been moved away from the chromosome surface. Without this removal, NE fragments could delay kinetochore capturing for about 10 min, the time required for their complete disassembly. Mechanical checkpoint and kinetochore peeling functions are not mutually exclusive and reinforce the view that formation of the mitotic spindle and nuclear disassembly are two intertwined and highly coordinated processes.

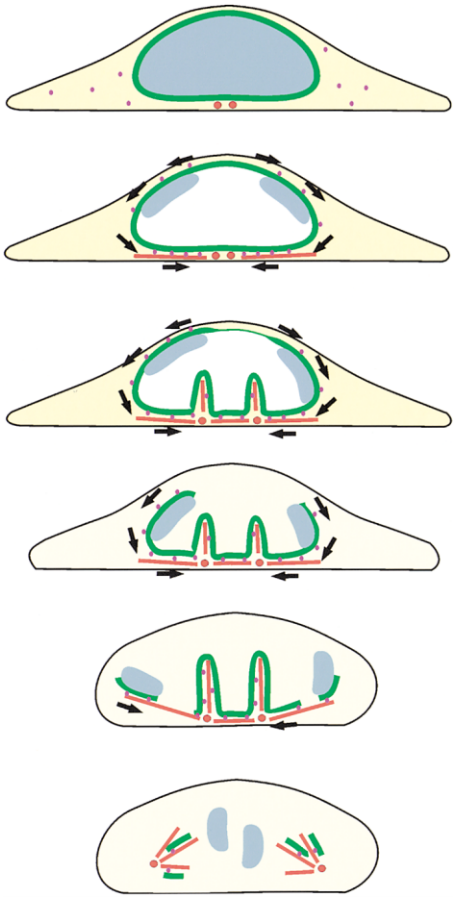

Figure 7. Model of NEBD by Microtubule-Induced Tearing

Schematic drawing depicting the process of nuclear lamina stretching and tearing by microtubule-mediated pulling on the NE surface. Chromosomes (blue), nuclear lamina (green), microtubules and centrosomes (red), and a minus-end-directed motor (purple) are shown. Black arrows represent the force exerted on the NE. Yellow cytoplasm turns light after mixing with nucleoplasm at NEBD. For details see text.

A Model for NEBD

We propose a model of NEBD where immobilization of a minus-end-directed microtubule motor such as dynein on the NE surface accounts for the generation of tension and folds in the NE and NE tearing as well as the subsequent movement of NE fragments to the spindle poles (Figure 7). In late G2, dynein would become immobilized on the surface of the NE, presumably by binding to NPCs. The motor would serve to attach newly nucleated spindle microtubules to the NE. Minus-end-directed motion would start to create pulling forces on the NE surface toward the centrosome. These forces would become stronger with increasing length and number of spindle microtubules and push NE material toward the centrosomes, creating folds. Distal from centrosomes,

Bars: 5 μm. (E) shows the track of the fragment over time. The red dots correspond to the frames shown in (D). Velocity is indicated for sustained motion along the path.

(F) Instantaneous speed histogram of 47 fragment movements, recorded in 17 different $NRK_{H2B\text{-}CFP}$ cells transiently expressing lamin B1-YFP. Note that the speed can reach up to 1.8 μm/s.

the result would be stretching and finally tearing of the lamina. After NEBD, NE fragments would be pulled away from chromosomes by dynein. In our model, NEBD is caused by tearing of the nuclear lamina, which we have shown to correspond to the site of permeabilization. However, due to the resolution limit of our imaging system, we can not exclude that a local lamina or NPC disassembly event below 0.5 μm in size preceded tearing. Our model is seemingly different from observations in starfish, where localized changes of NPC permeability were suggested to be the first step in NEBD (Terasaki et al., 2001). In addition, studies on late *C. elegans* embryos also suggested that the nucleoporin p62 is lost from the NE before lamins and INM proteins (Lee et al., 2000). We have shown here that a nucleoporin stably associated with the NPC, such as POM121 (Daigle et al., 2001), does not disassemble, and that NPCs are able to exclude a 500 kDa dextran before hole formation. Nevertheless, NPCs may already have altered properties and/or composition regarding other nucleoporins or smaller molecules at this time, as a recent study in *Drosophila* suggests that NPC disassembly occurs in discrete steps (Kiseleva et al., 2001). Our model provides an explanation for the site of appearance and spreading of gaps by mechanical forces. We speculate that this mechanism could act in concert with biochemical changes of the NPCs and certain INM proteins such as LBR to result in nuclear disassembly.

Experimental Procedures

Supplemental Data

Supplemental Figures and Movies can be found at http://www.cell.com/cgi/content/full/108/1/83/DC1.

Cell Lines, Cell Culture, Microinjection, Antibodies, and Synchronization

All experiments were performed in NRK cells cultured in complete DMEM (DMEM, 10% FCS, 2 mM glutamine, 100 U/ml streptomycin, 100 μg/ml penicillin). NRK clones stably expressing histone 2B-CFP, LBR-YFP, and α-tubulin-YFP were obtained and maintained as described (Daigle et al., 2001). For microscopy and microinjection, cells were cultured in #1 LabTekII chambered coverglasses (LabTek, Naperville, IL) maintained at 37°C (Daigle et al., 2001). In some cases, 0.2 μg/ml Hoechst 33342 was used to label DNA in vivo. Transfection was with FuGene 6 (Roche, Mannheim, Germany). Microinjection was with a Femtojet/Injectman micromanipulator (Eppendorf, Hamburg, Germany). Mitotic cells were injected with constant flow by gently penetrating the cell surface manually with a micropipette pulled on a P97 Flaming/Brown puller (Sutter Instr., Novato, CA) from GC120TF-10 glass capillaries (Harvard Apparatus Ltd., Kent, UK).

Mouse anti α-tubulin antibodies CDM1A and anti γ-tubulin GTU-88 were from Sigma (St. Louis, MO). 500 kDa amino dextran (Molecular Probes, Eugene, OR) was labeled with Cy5 using the fluorolink-Ab Cy5 labeling kit (Amersham Biosciences, Uppsala, Sweden). Free dye was removed by a Nanosep 30K Omega spin column (Pall Gelman, Ann Arbor, MI). Nocodazole (Sigma) was used at 1 μg/ml by adding a prewarmed 2× stock solution in medium to the cells on the microscope stage. For immunofluorescence, cells grown on #1 coverslips were rapidly transferred from 37°C to −20°C methanol at the indicated times after nocodazole addition. Synchronization was by arresting cells 24 or 48 hr posttransfection for 15 hr in 0.5 μg/ml aphidicolin, followed by a 7 hr release in complete medium. Individual prophase cells were selected from the synchronized population on the confocal microscope.

DNA Constructs

H2B-CFP, LBR-GFP, LBR-YFP, GFP-lamin B1, and POM121-3GFP have been described (Daigle et al., 2001; Ellenberg and Lippincott-Schwartz, 1999; Ellenberg et al., 1997). α-tubulin-YFP was made by replacing the GFP coding sequence of α-tubulin-GFP (Clontech Inc., Palo Alto, CA) with YFP from pEYFP-N1 (Clontech). C/YFP-lamin B1 was made by subcloning the lamin B1 cDNA from GFP-lamin B1 into pEYFP-C3 (Clontech) as described (Daigle et al., 2001). LAP2β-GFP and LAP2β-YFP were made by placing the coding sequence of rat LAP2β from clone pBS4b (Furukawa et al., 1995) as a BamHI fragment downstream of GFP or YFP in the BglII site of pEGFP-C1 or pEYFP-C1 (Clontech).

4D Imaging and Photobleaching

The 4D imaging system used has been described in detail elsewhere (Gerlich et al., 2001). Briefly, it consisted of a customized LSM 510 confocal microscope fitted with a z-scanning stage, ultrasensitive PMTs (Carl Zeiss, Göttingen, Germany), a Kr 413 nm laser (Coherent GmbH, Dieburg, Germany), and custom dichroics and emission filters (Chroma Inc., Brattleboro, VT) for fluorescent protein imaging. A typical z stack was 512 × 512 × 15 acquired with a PlanApochromat 63× NA 1.4 oil DIC objective (Carl Zeiss), a field width half maximum of 1.5 μm at a 1 μm step size, and could be acquired within 1.5 s. In this manner the entire cell volume was quantitatively accessible in 3D over time. Only images from cells that completed mitosis normally were used for subsequent analysis. Sequences shown are representative examples of 5–10 independent experiments.

FRAP experiments were performed on the LSM 510, essentially as described (Daigle et al., 2001; Ellenberg et al., 1997; Zaal et al., 1999). For pattern bleaching, a grid bleach mask was defined in the LSM 2.8 software using the inbuilt multiple ROI definition. The grid lines were 0.4 μm × 35 μm and intersected every 4 μm. This mask was bleached in two image planes centered on the lower and upper nuclear surface, respectively, within 10 s.

Image Segmentation, Reconstruction, and Quantitation

Quantitative 4D data analysis was carried out as described (Gerlich et al., 2001). Briefly, single images were filtered by anisotropic diffusion and segmented, and the binarized object representation was used to measure volume over time. Gray values in the segmented area of original images were measured after background subtraction to determine the concentration of GFP-labeled protein in a compartment. Isosurface reconstructions of 4D data sets were with Amira (Template Graphics Software Inc., San Diego, CA). For data sets where automatic segmentation failed due to noise, structures were identified manually in maximum intensity projections and background subtracted, and total or mean fluorescence was measured using the public domain programs NIH Image 1.62 (http://rsb.info.nih.gov/nih-image/) and Image J (http://rsb.info.nih.gov/ij/). Normalization and plotting of numerical data was in Microsoft Excel (Microsoft Corp., Redmond, WA). Other normalizations are described in the figure legends.

Chromosome condensation was measured by plotting the fluorescence intensity histograms of maximum intensity projections of 4D sequences of H2B-CFP expressing cells from prophase to metaphase (Figure 3D). The condensation state, defined as the most frequent intensity, was determined after smoothing the histogram by fitting it with a 9-degree polynomial. The rate of condensation was defined as the relative change of condensation state over time (Figure 3F). Nuclear volume measurements after NEBD (Figure 3B) were performed by closing the discontinuities in the lamina signal with the smallest possible surface connection. Quantitation was stopped when the lamina surface was too fragmented for efficient closing (Figure 3, 0:30). Multichannel digital images of live cells are shown systematically with nuclear envelope markers in green, and all other markers (chromosomes, tubulin, dextran) in red for best visualization of the differentially labeled structures.

Acknowledgments

The authors would like to thank Gaëlle Kerjan for help with the FRAP experiments, Nihal Altan for sharing synchronization protocols, Kazu Furukawa for the generous gift of the LAP2β cDNA, Mark Terasaki for continuous stimulating discussions, Pétér Lénart for help with

Figure 7, and Iain Mattaj, Ernst-Ludwig Florin, and Elisa Izaurralde for critical reading of the manuscript.

J.B. was supported by a fellowship through EMBL's International Ph.D. Programme. R.E. acknowledges the BioFuture grant by BMBF (11880 A) and support by the DFG (Ei358/2-1 and FOR 240).

Received July 17, 2001; revised December 10, 2001.

References

Alberts, B. (1994). Molecular Biology of the Cell, 3rd edition (New York: Garland Pub.).

Bajer, A., and Molé-Bajer, J. (1969). Formation of spindle fibers, kinetochore orientation, and behavior of the nuclear envelope during mitosis in endosperm. Chromosoma *27*, 448–484.

Belgareh, N., Rabut, G., Bai, S.W., van Overbeek, M., Beaudouin, J., Daigle, N., Zatsepina, O.V., Pasteau, F., Labas, V., Fromont-Racine, M., et al. (2001). An evolutionarily conserved NPC subcomplex, which redistributes in part to kinetochores in mammalian cells. J. Cell Biol. *154*, 1147–1160.

Buendia, B., and Courvalin, J.C. (1997). Domain-specific disassembly and reassembly of nuclear membranes during mitosis. Exp. Cell Res. *230*, 133–144.

Busson, S., Dujardin, D., Moreau, A., Dompierre, J., and De Mey, J.R. (1998). Dynein and dynactin are localized to astral microtubules and at cortical sites in mitotic epithelial cells. Curr. Biol. *8*, 541–544.

Courvalin, J.C., Segil, N., Blobel, G., and Worman, H.J. (1992). The lamin B receptor of the inner nuclear membrane undergoes mitosis-specific phosphorylation and is a substrate for p34cdc2-type protein kinase. J. Biol. Chem. *267*, 19035–19038.

Daigle, N., Beaudouin, J., Hartnell, L., Imreh, G., Hallberg, E., Lippincott-Schwartz, J., and Ellenberg, J. (2001). Nuclear pore complexes form immobile networks and have a very low turnover in live mammalian cells. J. Cell Biol. *154*, 71–84.

Drummond, S., Ferrigno, P., Lyon, C., Murphy, J., Goldberg, M., Allen, T., Smythe, C., and Hutchison, C.J. (1999). Temporal differences in the appearance of NEP-B78 and an LBR-like protein during Xenopus nuclear envelope reassembly reflect the ordered recruitment of functionally discrete vesicle types. J. Cell Biol. *144*, 225–240.

Ellenberg, J., and Lippincott-Schwartz, J. (1997). Fluorescence Photobleaching Techniques. In Cells: A Laboratory Manual, D. Spector, R. Goldman, and L. Leinwand, eds. (Cold Spring Harbor, Cold Spring Harbor Laboratory Press), pp. 79.1–79.23.

Ellenberg, J., and Lippincott-Schwartz, J. (1999). Dynamics and mobility of nuclear envelope proteins in interphase and mitotic cells revealed by green fluorescent protein chimeras. Methods *19*, 362–372.

Ellenberg, J., Siggia, E.D., Moreira, J.E., Smith, C.L., Presley, J.F., Worman, H.J., and Lippincott-Schwartz, J. (1997). Nuclear membrane dynamics and reassembly in living cells: targeting of an inner nuclear membrane protein in interphase and mitosis. J. Cell Biol. *138*, 1193–1206.

Favreau, C., Worman, H.J., Wozniak, R.W., Frappier, T., and Courvalin, J.C. (1996). Cell cycle-dependent phosphorylation of nucleoporins and nuclear pore membrane protein Gp210. Biochemistry *35*, 8035–8044.

Fey, E.G., Wan, K.M., and Penman, S. (1984). Epithelial cytoskeletal framework and nuclear matrix-intermediate filament scaffold: three-dimensional organization and protein composition. J. Cell Biol. *98*, 1973–1984.

Foisner, R., and Gerace, L. (1993). Integral membrane proteins of the nuclear envelope interact with lamins and chromosomes, and binding is modulated by mitotic phosphorylation. Cell *73*, 1267–1279.

Furukawa, K., Pante, N., Aebi, U., and Gerace, L. (1995). Cloning of a cDNA for lamina-associated polypeptide 2 (LAP2) and identification of regions that specify targeting to the nuclear envelope. EMBO J. *14*, 1626–1636.

Georgatos, S.D., Pyrpasopoulou, A., and Theodoropoulos, P.A. (1997). Nuclear envelope breakdown in mammalian cells involves stepwise lamina disassembly and microtubule-drive deformation of the nuclear membrane. J. Cell Sci. *110*, 2129–2140.

Gerace, L., and Blobel, G. (1980). The nuclear envelope lamina is reversibly depolymerized during mitosis. Cell *19*, 277–287.

Gerace, L., and Burke, B. (1988). Functional organization of the nuclear envelope. Annu. Rev. Cell Biol. *4*, 335–374.

Gerlich, D., Beaudouin, J., Gebhard, M., Ellenberg, J., and Eils, R. (2001). 4-D imaging and quantitative reconstruction to analyze complex spatiotemporal processes in live cells. Nat. Cell Biol. *3*, 852–855.

Goldberg, M.W., and Allen, T.D. (1995). Structural and functional organization of the nuclear envelope. Curr. Opin. Cell Biol. *7*, 301–309.

Gönczy, P., Pichler, S., Kirkham, M., and Hyman, A.A. (1999). Cytoplasmic dynein is required for distinct aspects of MTOC positioning, including centrosome separation, in the one cell stage Caenorhabditis elegans embryo. J. Cell Biol. *147*, 135–150.

Gruenbaum, Y., Wilson, K.L., Harel, A., Goldberg, M., and Cohen, M. (2000). Review: nuclear lamins—structural proteins with fundamental functions. J. Struct. Biol. *129*, 313–323.

Hamaguchi, Y., Satoh, S.K., and Hamaguchi, M.S. (1993). Projections of the nuclear envelope into the nucleus prior to its breakdown. Bioimages *1*, 129–136.

Heald, R., and McKeon, F. (1990). Mutations of phosphorylation sites in lamin A that prevent nuclear lamina disassembly in mitosis. Cell *61*, 579–589.

Kiseleva, E., Rutherford, S., Cotter, L.M., Allen, T.D., and Goldberg, M.W. (2001). Steps of nuclear pore complex disassembly and reassembly during mitosis in early Drosophila embryos. J. Cell Sci. *114*, 3607–3618.

Lee, K.K., Gruenbaum, Y., Spann, P., Liu, J., and Wilson, K.L. (2000). C. elegans nuclear envelope proteins emerin, MAN1, lamin, and nucleoporins reveal unique timing of nuclear envelope breakdown during mitosis. Mol. Biol. Cell *11*, 3089–3099.

Longo, F.J. (1972). An ultrastructural analysis of mitosis and cytokinesis in the zygote of the sea urchin, Arbacia punctulata. J. Morphol. *138*, 207–238.

Ma, S., Trivinos-Lagos, L., Graf, R., and Chisholm, R.L. (1999). Dynein intermediate chain mediated dynein-dynactin interaction is required for interphase microtubule organization and centrosome replication and separation in Dictyostelium. J. Cell Biol. *147*, 1261–1274.

Macaulay, C., Meier, E., and Forbes, D.J. (1995). Differential mitotic phosphorylation of proteins of the nuclear pore complex. J. Biol. Chem. *270*, 254–262.

Maniotis, A.J., Chen, C.S., and Ingber, D.E. (1997). Demonstration of mechanical connections between integrins, cytoskeletal filaments, and nucleoplasm that stabilize nuclear structure. Proc. Natl. Acad. Sci. USA *94*, 849–854.

Marshall, I.C.B., and Wilson, K.L. (1997). Nuclear envelope assembly after mitosis. Trends Cell Biol. *7*, 69–74.

Newport, J., and Spann, T. (1987). Disassembly of the nucleus in mitotic extracts: membrane vesicularization, lamin disassembly, and chromosome condensation are independent processes. Cell *48*, 219–230.

Paweletz, N., and Lang, U. (1988). Fine structural studies of early mitotic stages in untreated and nocodazole-treated HeLa cells. Eur. J. Cell Biol. *47*, 334–345.

Peter, M., Nakagawa, J., Doree, M., Labbe, J.C., and Nigg, E.A. (1990). In vitro disassembly of the nuclear lamina and M phase-specific phosphorylation of lamins by cdc2 kinase. Cell *61*, 591–602.

Peter, M., Heitlinger, E., Haner, M., Aebi, U., and Nigg, E.A. (1991). Disassembly of in vitro formed lamin head-to-tail polymers by CDC2 kinase. EMBO J. *10*, 1535–1544.

Pfaller, R., Smythe, C., and Newport, J.W. (1991). Assembly/disassembly of the nuclear envelope membrane: cell cycle-dependent binding of nuclear membrane vesicles to chromatin in vitro. Cell *65*, 209–217.

Plamann, M., Minke, P.F., Tinsley, J.H., and Bruno, K.S. (1994). Cytoplasmic dynein and actin-related protein Arp1 are required for nor-

mal nuclear distribution in filamentous fungi. J. Cell Biol. *127*, 139–149.

Presley, J.F., Cole, N.B., Schroer, T.A., Hirschberg, K., Zaal, K.J., and Lippincott-Schwartz, J. (1997). ER-to-Golgi transport visualized in living cells. Nature *389*, 81–85.

Reinsch, S., and Gönczy, P. (1998). Mechanisms of nuclear positioning. J. Cell Sci. *111*, 2283–2295.

Robbins, E., and Gonatas, N.K. (1964). The ultrastructure of a mammalian cell during the mitotic cell cycle. J. Cell Biol. *21*, 429–463.

Robinson, J.T., Wojcik, E.J., Sanders, M.A., McGrail, M., and Hays, T.S. (1999). Cytoplasmic dynein is required for the nuclear attachment and migration of centrosomes during mitosis in Drosophila. J. Cell Biol. *146*, 597–608.

Rolls, M.M., Stein, P.A., Taylor, S.S., Ha, E., McKeon, F., and Rapoport, T.A. (1999). A visual screen of a GFP-fusion library identifies a new type of nuclear envelope membrane protein. J. Cell Biol. *146*, 29–44.

Salina, D., Bodoor, K., Eckley, D.M., Schroer, T.A., Rattner, J.B., and Burke, B. (2002). Cytoplasmic dynein as a facilitator of nuclear envelope breakdown. Cell *108*, 97–107.

Sasagawa, S., Yamamoto, A., Ichimura, T., Omata, S., and Horigome, T. (1999). In vitro nuclear assembly with affinity-purified nuclear envelope precursor vesicle fractions, PV1 and PV2. Eur. J. Cell Biol. *78*, 593–600.

Stick, R., Angres, B., Lehner, C.F., and Nigg, E.A. (1988). The fates of chicken nuclear lamin proteins during mitosis: evidence for a reversible redistribution of lamin B2 between inner nuclear membrane and elements of the endoplasmic reticulum. J. Cell Biol. *107*, 397–406.

Terasaki, M. (2000). Dynamics of the endoplasmic reticulum and golgi apparatus during early sea urchin development. Mol. Biol. Cell *11*, 897–914.

Terasaki, M., Campagnola, P., Rolls, M.M., Stein, P.A., Ellenberg, J., Hinkle, B., and Slepchenko, B. (2001). A new model for nuclear envelope breakdown. Mol. Biol. Cell *12*, 503–510.

Ward, G.E., and Kirschner, M.W. (1990). Identification of cell cycle-regulated phosphorylation sites on nuclear lamin C. Cell *61*, 561–577.

Wilson, K.L. (2000). The nuclear envelope, muscular dystrophy and gene expression. Trends Cell Biol. *10*, 125–129.

Yamamoto, A., West, R.R., McIntosh, J.R., and Hiraoka, Y. (1999). A cytoplasmic dynein heavy chain is required for oscillatory nuclear movement of meiotic prophase and efficient meiotic recombination in fission yeast. J. Cell Biol. *145*, 1233–1249.

Yang, L., Guan, T., and Gerace, L. (1997). Integral membrane proteins of the nuclear envelope are dispersed throughout the endoplasmic reticulum during mitosis. J. Cell Biol. *137*, 1199–1210.

Ye, Q., and Worman, H.J. (1994). Primary structure analysis and lamin B and DNA binding of human LBR, an integral protein of the nuclear envelope inner membrane. J. Biol. Chem. *269*, 11306–11311.

Zaal, K.J.M., Smith, C.L., Polishchuk, R.S., Altan, N., Cole, N.B., Ellenberg, J., Hirschberg, K., Presley, J.F., Roberts, T.H., Siggia, E., et al. (1999). Golgi membranes are absorbed into and reemerge from the ER during mitosis. Cell *99*, 589–601.

Zatsepina, O.V., Polyakov, V.Y., and Chentsov, Y.S. (1977). Some structural aspects of the fate of the nuclear envelope during mitosis. Eur. J. Cell Biol. *16*, 130–144.